Article

Substrate Signal Inhibition in Raman Analysis of Microplastic Particles

Ahmed A. Elsayed, Ahmed M. Othman, Yasser M. Sabry, Frédéric Marty, Haitham Omran, Diaa Khalil, Ai-Qun Liu, and Tarik Bourouina*

Read Online

ACCESS | Metrics & More | Article Recommendations

ABSTRACT: In Raman analysis, the substrate material serves very often for signal enhancement, especially when metallic surfaces are involved; however, in other cases, the substrate has an opposite effect as it is the source of a parasitic signal preventing the observation of the sample material of interest. This is particularly true with the advent of microfluidic devices involving either silicon or polymer surfaces. On the other hand, in a vast majority of Raman experiments, the analysis is made on a horizontal support holding the sample of interest. In our paper, we report that a simple tilting of the supporting substrate, in this case, silicon, can drastically decrease and eventually inhibit the Raman signal of the substrate material, leading to an easier observation of the target analyte of the sample, in this case, microplastic particles. This effect is very pronounced especially when looking for tiny particles. Explanation of this trend is provided thanks to a supporting experiment and further numerical simulations that suggest that the lensing effect of the particles plays an important role. These findings may be useful for Raman analysis of other microscale particles having curved shapes, including biological cells.
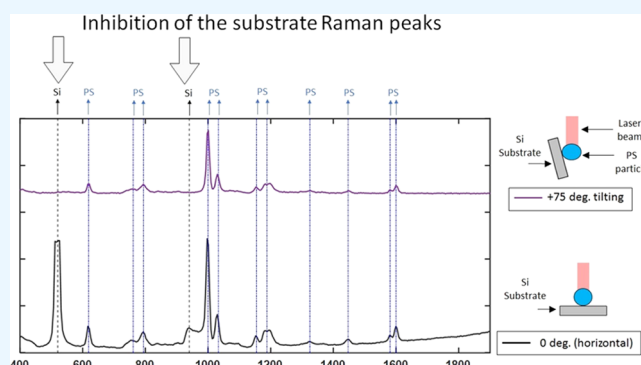
INTRODUCTION

Raman spectroscopy is a key analytical tool that is used to determine the chemical nature of a sample, thanks to light—matter interaction with specific spectral signatures, which facilitates the remote identification of a wide variety of materials. It is reliable, nondestructive, fast, and suitable for a wide scale of dimensions.[1−6] However, the weak Raman signal can be a disadvantage, requiring optimized and expensive instrumentation that can limit the scope of applications.[1,3,4] This is most evident in applications where the analysis of individual small-sized particles (in the micro-/nanoscale) is required, such as microplastic identification,[7−9] cell analysis,[10,11] and airborne-particle analysis.[12,13] This is further impaired by the presence of other parasitic signals that can mask the target signal of the analyte, such as the Raman scattering peaks of the substrate on which the analyte particles reside. For instance, analyzing microplastic particles on a silicon (Si) substrate can be affected by the strong Si Raman peaks, including the main peak at nearly 520.6 cm^{-1} and the broader (but less intense) second-order peak at around 940 cm^{-1}.[14,15] This is especially evident when analyzing smaller plastic particles (<10 μm) of a much weaker Raman signal, such as PMMA compared to Si.[16] Similarly, the analysis of cells and biological samples requires the characterization of different substrates to ensure minimal interference of their spectral signal with the analyte,[17,18] which introduces

additional effort to the analysis process and can pose constraints on the usable substrates.

In this work, an approach to get rid of the parasitic Raman signal of the substrate is proposed by simply tilting the substrate. To demonstrate this, model plastic microparticles are measured on a Si substrate that is tilted with different angles, resulting in a noticeable decrease in intensity of the Si Raman peaks as the tilting angle increases. The parasitic Si peaks almost completely diminish at large angles (of nearly 75°), while the plastic microparticles Raman peaks remain measurable.

MATERIALS AND METHODS

Raman Spectrometer. The compact Raman spectrometer used in this work is the model C13560 produced by Hamamatsu Photonics (Japan). It utilizes a laser diode of wavelength 785 nm capable of providing an optical power up to 15 mW, with the smallest spot size of around 20 μm diameter. This spectrometer measures the Raman shift range of 400−1850 cm^{-1} with a
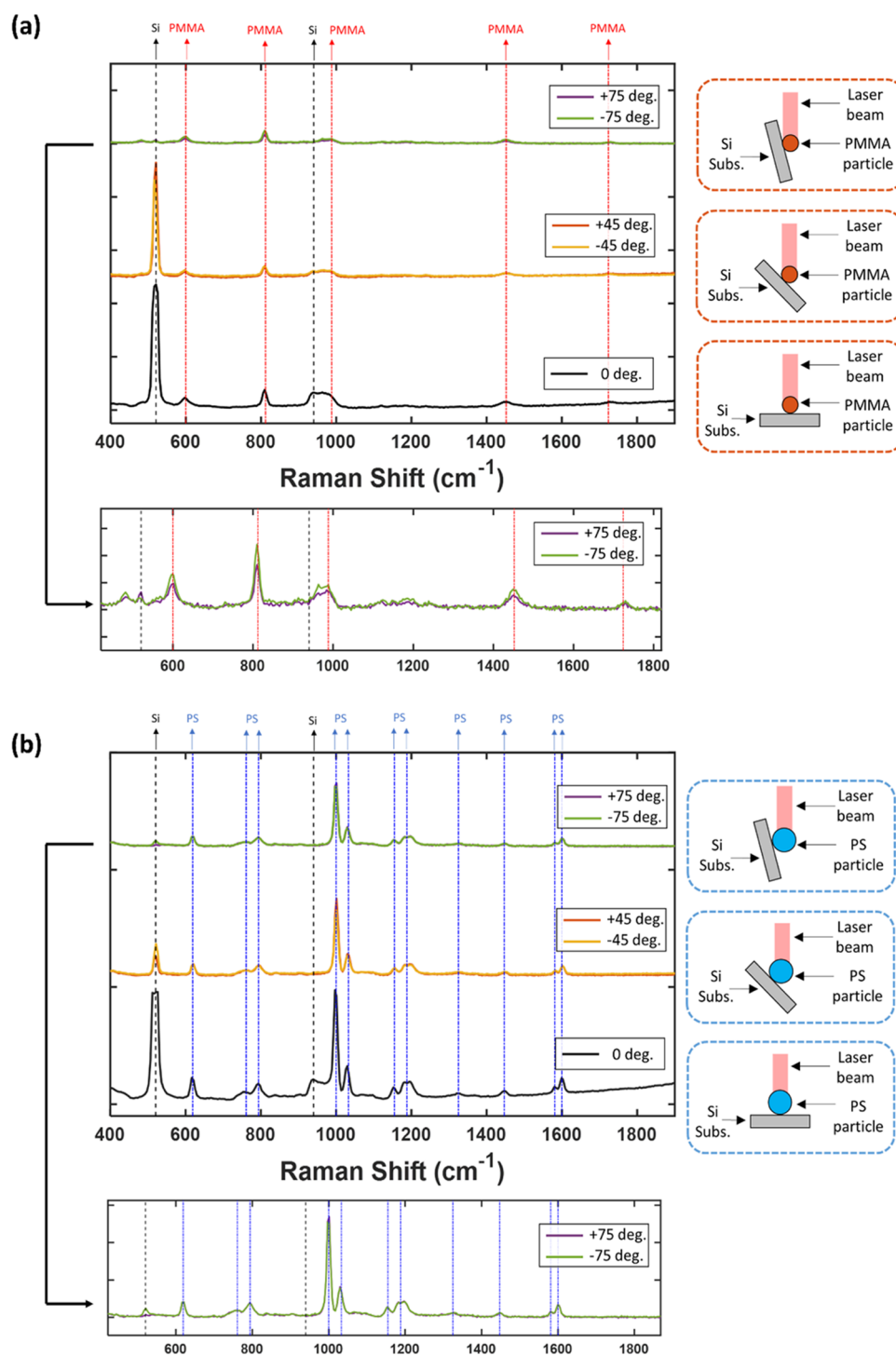
Figure 1. (a) Raman spectra for single PMMA 40 μm particles at different substrate tilt angles. The theoretical positions of the Raman peaks of Si and PMMA are shown as vertical black and red lines, respectively. (b) Raman spectra for single PS 80 μm particles at different substrate tilt angles. The theoretical positions of the Raman peaks of Si and PS are shown as vertical black and blue lines, respectively. The case of 75° tilting is replotted below both figure parts at a larger scale to highlight the diminishing of the Si peaks.

spectral resolution of 10 cm^{-1}. The spectrometer has compact dimensions of $8 \times 6 \times 1.25$ cm^3.

Model Plastic Particles. The model particles measured in this work are spherical plastic particles of two types and diameters, polystyrene (PS) 80 μm and poly(methyl methacrylate) (PMMA) 40 μm provided by Microbeads AS (Norway).

Setup. The setup used to conduct the measurements consists of a small Si substrate fixed to a rotating arm that can rotate around its axis, hence tilting the Si substrate with respect to the laser illumination of the spectrometer. First, the model particles are spread on the substrate and the distance between the horizontal substrate and the spectrometer is adjusted to optimize the Raman signal intensity. Then, measurements of
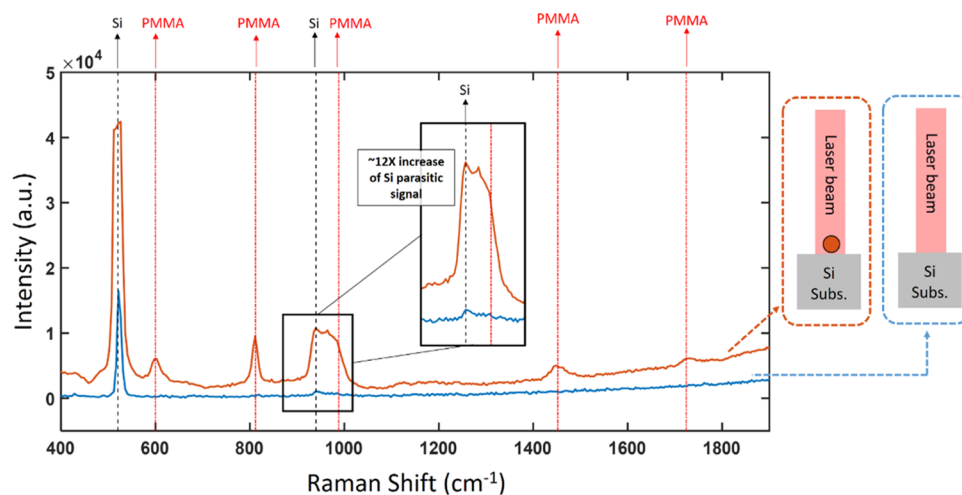
Figure 2. Raman parasitic peaks of the Si substrate, which increases in intensity beneath spherical particles.
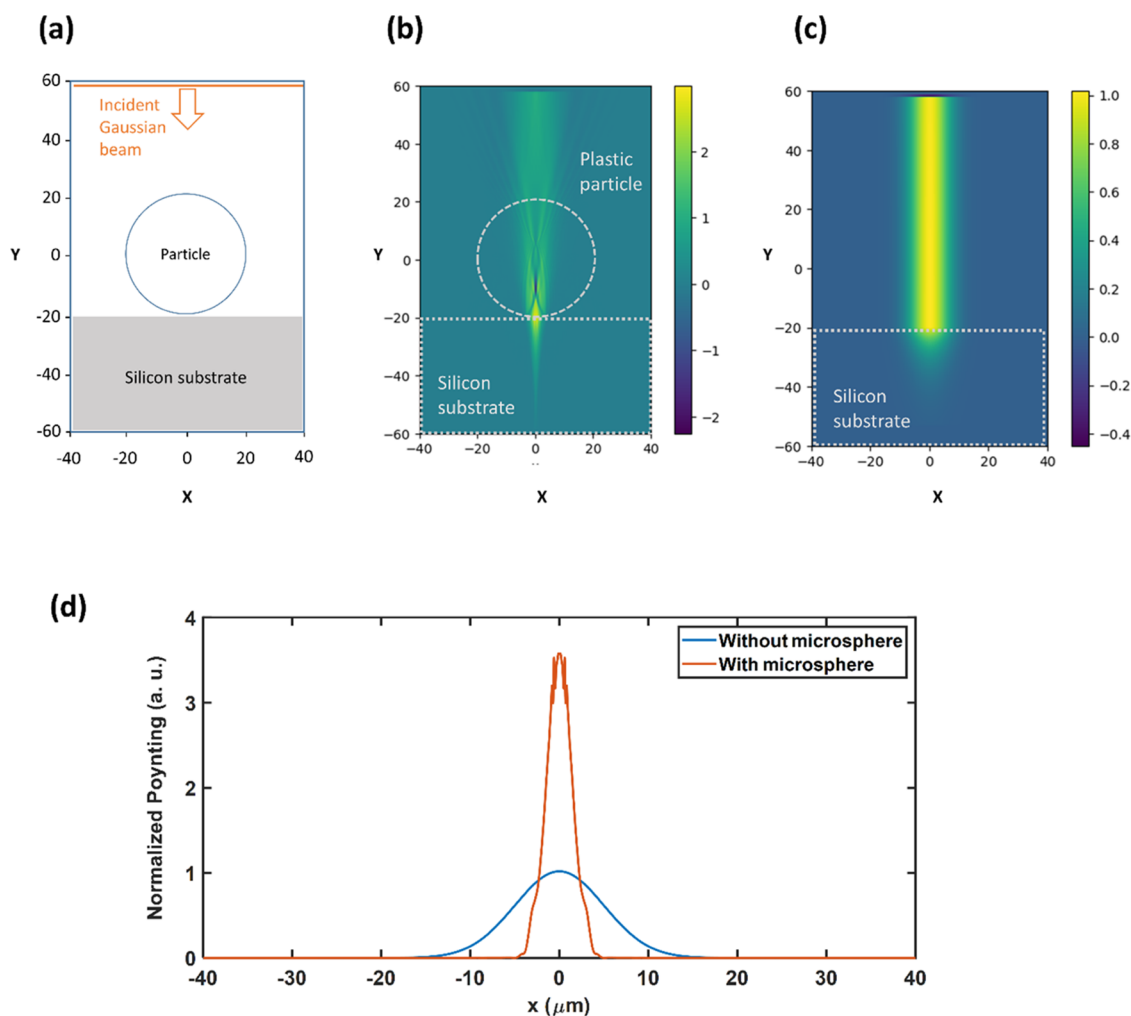

Figure 3. (a) Schematic showing the FDTD (Meep) simulation setup for a Gaussian beam incident on a plastic particle placed on a Si substrate. Dimensions are shown in μm. (b) The Poynting vector obtained using Meep FDTD software for the case with the PMMA particle, and (c) without the PMMA particle showing the focusing effect introduced by the particle on the Si substrate beneath it. (d) Normalized Poynting vector magnitude at the substrate edge with and without the presence of the microsphere.

single plastic particles are taken at different angles of 0, ±45, and ±75°.

FDTD Simulations. Finite-difference time-domain (FDTD) simulations are conducted using Meep simulation software,

which is a free and open-source package for electromagnetic simulations.[19] The simulation is meshed in cubic cells with a side length of 0.02 μm. The boundaries are perfectly matched layers at all sides of the structure (having a thickness of 2 μm).
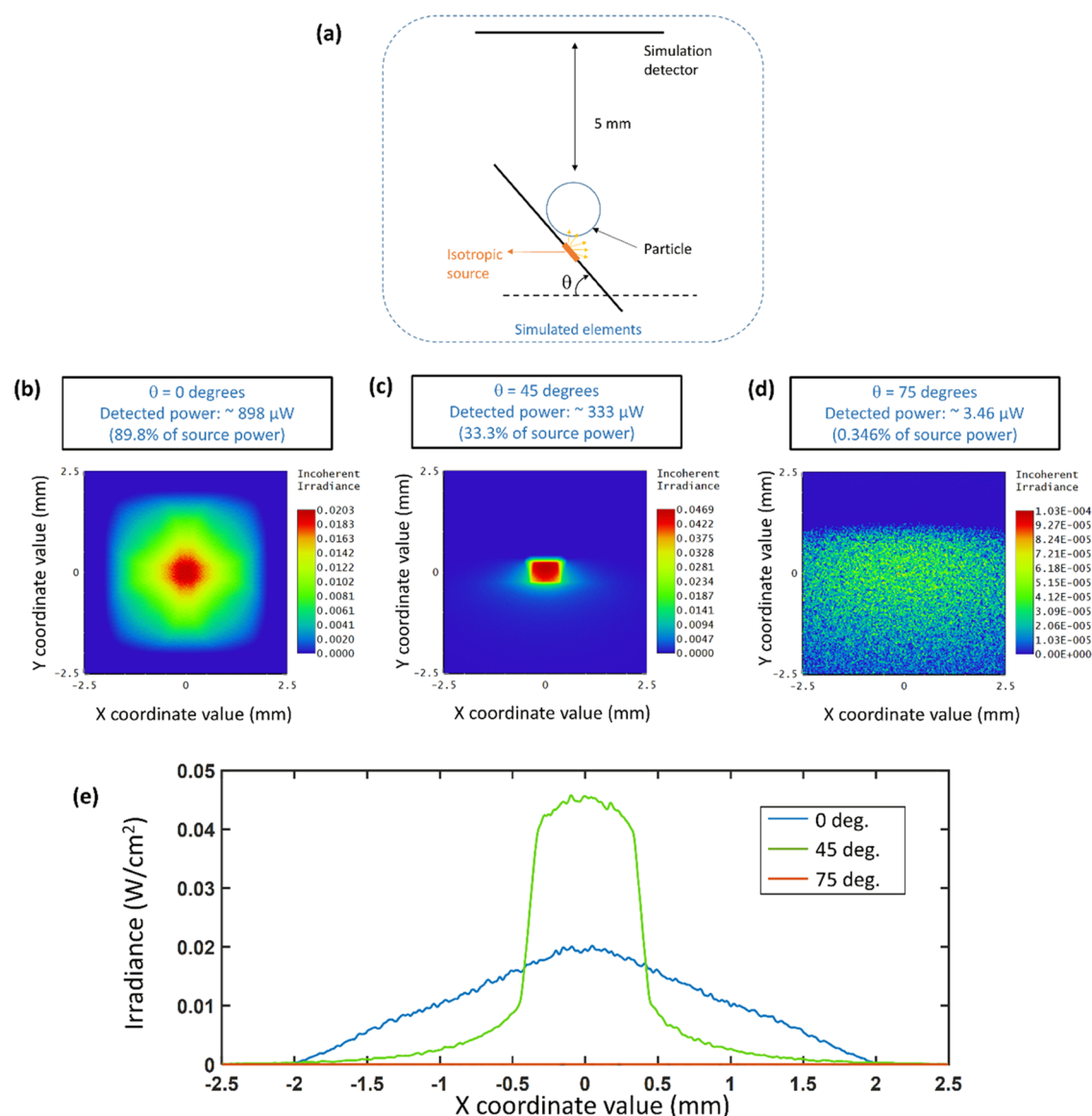
Figure 4. (a) Schematic showing the ray-optics (Zemax OpticStudio) simulation setup of an isotropic source within the silicon substrate beneath the particle to get an estimation of the amount of power (emulating the silicon Raman signal) reaching the detector for different tilt angles given the possible shadowing effect by the spherical particle. The simulation results show the irradiance on the detector for different substrate tilt angles of (b) 0°, (c) 45°, and (d) 75°. The irradiance curves across a horizontal cross section are also given and compared in part (e).

Ray-Optics Simulations. The ray-optics simulations are conducted using Zemax OpticStudio (ANSYS) ray tracing software. The simulations are set up to mimic as closely as possible the practical measurements (in terms of spot size, particle size, particle material, substrate tilt angles, distances between different elements, etc.).

RESULTS

The Raman spectrum is obtained for a single spherical particle targeted with the laser spot and lying on a Si substrate. The measurements are conducted while tilting the substrate at different angles. The first set of measurements includes targeting a single PMMA 40 μm particle, and the obtained spectra are shown in Figure 1a. The laser power used is 15 mW which is the maximum attainable by the laser diode of the spectrometer. For the case of a horizontal substrate (0° tilting), strong Si peaks can be noticed at nearly 520.6 and 940 cm^{-1}, in addition to the PMMA peaks at around 600, 812, 988, 1452, and 1724

cm^{-1}.[14,15,20] However, for a larger tilt angle of ±45°, the Si peaks are of a smaller intensity. It should be noted that the Si main peak (at 520.6 cm^{-1}) is saturating the detector (especially in the 0° case) so the decrease in its intensity for larger tilt angles is not as pronounced as the second-order peak of Si (at nearly 940 cm^{-1}). For the largest tilt angle of ±75°, it is noticed that the Si peaks almost completely disappear from the spectra, while the peaks of PMMA are still visible and align very well with the theoretical positions; hence, the parasitic effect of the Si peaks is removed from the background, emphasizing the analyte spectrum (which is the PMMA particle). It should be noted that a number of particles are spread on the Si substrate and that the measured particle at different substrate tilt angles is not necessarily the same (however, the particles have identical physical and chemical properties). Similar measurements are conducted on single PS 80 μm particles (shown in Figure 1b), where, in this case, the PS peaks are seen at nearly 619, 761, 794, 1000, 1033, 1155, 1188, 1325, 1447, 1581, and 1600 cm^{-1}.[21] As the Si

substrate tilt angle increases, the same effect is noticed where the Si peaks diminish, leaving only the PS peaks.

In a second experiment, we compared the Raman spectra of the Si substrate with and without the presence of a particle (where a PMMA 40 μm particle is used). The results are shown in Figure 2. The Si Raman peaks are noticed to have moderate intensity for the first case of the bare substrate (shown as the blue curve). For the case of the PMMA particle on top of the Si substrate (shown as the orange curve), there is a significant increase in the parasitic Raman peaks of Si. This increase in intensity is quantified to be about 12 times by comparing the second-order Raman peak (at around 940 cm^{-1}), where the main peak at 520.6 cm^{-1} causes saturation of the spectrometer detector and cannot be compared.

■ DISCUSSION

According to the results shown in Figure 1, it is very fortunate that the parasitic peaks of the Si substrate are inhibited by tilting. To understand the reasons for this trend, we have also to consider the result shown in Figure 2, which clearly shows that the presence of the microparticle leads to an enhancement of the substrate signal. Although this trend is unwanted and contrary to the conventional signal enhancement of the analyte, this result suggests that a lensing effect by the particle might occur, causing a concentration of the incident light on the Si substrate. Indeed, the geometrical shape of the particle can play an important role in the intensity of the parasitic signal of the Si substrate, where spherical or cylindrical particles can act as lenses focusing the incident laser spot on the substrate beneath and increasing the intensity of its corresponding Raman signal (which should be a linear increase).[6] This hypothesis is tested through simulations.

Simulations based on FDTD are conducted using Meep software, where a z linearly polarized Gaussian beam with a beam waist radius of 10 μm is incident on a 40 μm plastic (PMMA) sphere placed on a Si substrate, as shown in the schematic in Figure 3a, and the resulting Poynting vector ($-y$ component) magnitude is plotted. In these simulations, the 40 μm particle is centered on the origin; hence, the Si substrate edge is situated at $y = -20$ μm. It should be noted that the simulations are conducted in two dimensions (2D) due to computational limitations; hence, the simulated cross section in 2D will correspond to an infinite cylinder in 3D, but the expected focusing effect can still be qualitatively compared to the practical measurements.

The resulting Poynting vector shows that the spherical PMMA particle indeed has a focusing effect on the incident Gaussian beam, which is demonstrated in Figure 3b. The focusing effect is noticed as the intensity significantly increases beneath the particle at the Si substrate edge. Figure 3c shows the case without the PMMA sphere, where the incident Gaussian beam decays inside the Si substrate (whose edge is at $y = -20$ μm).

To better demonstrate the increase in the Poynting vector, a cross section along the x-axis is plotted at the Si substrate surface (at $y = -20$ μm) for the cases with and without the PMMA particle. The results are shown in Figure 3d, where it can be noticed that the PMMA sphere leads to an increase in the Poynting vector of nearly 3-fold at the Si substrate surface, at $x = 0$, which explains the increase noticed in the Si Raman peak obtained experimentally (and shown earlier in Figure 2). It should be noted that the lower intensity increase (3-fold) noticed in the simulations compared to the increase in the Si Raman peak (shown practically to be 12×) can be attributed to

conducting the simulations in 2D, while 3D simulations are expected to show better focusing of the incident beam in 3D beneath the particle.

Regarding the decrease and the vanishing of the Si peaks after tilting, this trend can be attributed to the shadowing effect that the particle has, where the Raman signal emitted from the Si substrate can be stopped from reaching the detector of the spectrometer by the particle that refracts/reflects rays away from it. However, this does not affect the Raman signal emitted from the particle itself given that there is no obstacle between the particle and the detector of the Raman spectrometer and given that the particle remains at a constant distance to the spectrometer and also due to the axial symmetry of the spherical particle. To test this hypothesis, simulations using ray-optics (Zemax OpticStudio software) with an isotropic source situated on the substrate beneath the particle (emulating the Raman signal emitted from the Si substrate in all directions) are conducted. These simulations help obtain a qualitative insight into the amount of power reaching the spectrometer detector at different substrate tilt angles given the particle shadowing effect. The presented simulations are conducted for a 40 μm PMMA particle, and an isotropic source emitting 1 mW, while the power is detected 5 mm away from the particle (similar to the practical setup). A schematic describing this simulation is shown in Figure 4a.

The simulation results are shown in Figure 4, which show the irradiance on the detector and the total power detected. It can be noticed that for a tilt angle of 0° (Figure 4b) most of the source power can reach the detector (nearly 898 μW, which constitutes 89.8% of the emitted power), and the irradiance pattern shows some collimation of the light rays due to the particle acting as a spherical lens with respect to the rays emitted from the isotropic source on the substrate right beneath it.

However, for a tilt angle of 45°, only 333 μW (33.3% of the emitted power) is detected (shown in Figure 4c). Another noticeable aspect is that the irradiance is higher compared to the previous case (of the 0° tilt angle) and the light rays are better collimated on the detector. This can be attributed to the isotropic source being placed on the substrate lying nearly at the focal point of the spherical particle (or lens) when it is tilted by 45°, causing the emitted rays to be better collimated (however, the total power is still less compared to the case of the 0° tilt angle).

Finally, for the largest tilt angle of 75°, most of the power is lost, where only 3.46 μW (constituting 0.346% of the emitted power) is detected, and the irradiance is orders of magnitude lower compared to previous cases (shown in Figure 4d). The irradiance curves for the different tilt angles are compared in Figure 4e. The results of these simulations confirm the assumption that the higher the tilt angle of the substrate, the less likely for the emitted signal to reach the detector due to the shadowing effect of the particle, which agrees with the measurements shown in Figure 1, where the Raman signal of the Si substrate diminishes for larger tilt angles, leaving only Raman peaks of the PMMA particle.

This approach of tilting the substrate to inhibit its Raman signal while maintaining the Raman signal of the particle (which is the analyte) is believed to be applicable for particles in the microscale (1 μm to hundreds of microns, using the appropriate instruments and setup), and it is validated through experiments and simulations for particles of different sizes (including 10, 20, 40, and 80 μm). The results of the larger particle sizes (40 and 80 μm) are presented in this work, especially that the obtained

Raman peaks for smaller particles are less pronounced given the rather low power of the Raman system used in our experiments (especially for PMMA) regardless of the tilting angle. It should be noted that the approach is applicable for the range of tilting angles of 0−90°, where a higher tilting angle results in a further decrease of the parasitic substrate Raman signal. However, higher tilting angles make the alignment of the spectrometer laser spot with the microparticle more difficult practically. It is also worth noting that particles with an arbitrary shape are expected to have a similar shadowing effect when the substrate is tilted, and the substrate's Raman signal is expected to decrease with tilting as well; however, the arbitrary shape of the particles could affect their own Raman signal reaching the detector, but considering nonspherical particles is a significantly different situation that was not studied in this work and requires more investigations.

While this work aims to suppress the Raman signal of the substrate material seen as a parasitic effect, one can note that in some other applications, it is the opposite that is desired, which is having an enhancement of the substrate Raman signal, which can have a useful effect where the microsphere can be used for the purpose of Raman enhancement of the substrate signal or another analyte beneath the particle,[22] but of course without any tilting of the substrate, as it would impair the enhancement.

CONCLUSIONS

While targeting the analysis of microplastic particles, it is found that a simple tilting of the supporting Si substrate can drastically decrease and eventually inhibit the Raman signal of Si, seen as a parasitic signal, especially when looking for tiny particles. Explanation of this trend is provided thanks to a supporting experiment, and further simulations that suggest that the lensing effect of the particles plays an important role. Our findings may be useful for Raman analysis of other microscale particles including biological cells.

AUTHOR INFORMATION

Corresponding Author
Tarik Bourouina − CNRS ESYCOM UMR 9007, Noisy-le-Grand, ESIEE, Université Gustave Eiffel, Paris 93162, France; orcid.org/0000-0003-2342-7149; Email: tarik.bourouina@esiee.fr

Authors
Ahmed A. Elsayed − CNRS ESYCOM UMR 9007, Noisy-le-Grand, ESIEE, Université Gustave Eiffel, Paris 93162, France; orcid.org/0000-0002-8000-2713

Ahmed M. Othman − CNRS ESYCOM UMR 9007, Noisy-le-Grand, ESIEE, Université Gustave Eiffel, Paris 93162, France; Si-Ware Systems, Cairo 11361, Egypt; orcid.org/0000-0003-2526-1082

Yasser M. Sabry − Si-Ware Systems, Cairo 11361, Egypt; Faculty of Engineering, Ain-Shams University, Cairo 11535, Egypt

Frédéric Marty − CNRS ESYCOM UMR 9007, Noisy-le-Grand, ESIEE, Université Gustave Eiffel, Paris 93162, France

Haitham Omran − Faculty of Information Engineering and Technology, Laboratory of Micro Optics, German University in Cairo, Cairo 11835, Egypt

Diaa Khalil − Si-Ware Systems, Cairo 11361, Egypt; Faculty of Engineering, Ain-Shams University, Cairo 11535, Egypt

Ai-Qun Liu − CNRS ESYCOM UMR 9007, Noisy-le-Grand, ESIEE, Université Gustave Eiffel, Paris 93162, France; School of Electrical and Electronic Engineering, Nanyang Technological University, Singapore 639798, Singapore; orcid.org/0000-0002-0126-5778

Complete contact information is available at:
https://pubs.acs.org/10.1021/acsomega.2c06536

Notes
The authors declare no competing financial interest.

REFERENCES
(1) Das, R. S.; Agrawal, Y. K. Raman spectroscopy: Recent advancements, techniques and applications. Vib. Spectrosc. 2011, 57, 163−176.
(2) Zoubir, A. Raman Imaging: Techniques and Applications; Springer-Verlag: Berlin, 2012.
(3) Gardiner, D. J.; Graves, P. R. Practical Raman Spectroscopy; Springer, 1989.
(4) Nakamoto, K.; Brown, C. W.Introductory Raman Spectroscopy; Elsevier, 1994.
(5) Ida, N.; Meyendorf, N.Handbook of Advanced Nondestructive Evaluation; Springer, 2020.
(6) Rzhevskii, A. Modern Raman Microscopy: Technique and Practice; Cambridge Scholars Publishing, 2021.
(7) Schymanski, D.; Goldbeck, C.; Humpf, H. U.; Fürst, P. Analysis of microplastics in water by micro-Raman spectroscopy: Release of plastic particles from different packaging into mineral water. Water Res. 2018, 129, 154−162.
(8) Oßmann, B. E.; Sarau, G.; Holtmannspötter, H.; Pischetsrieder, M.; Christiansen, S. H.; Dicke, W. l. Small-sized microplastics and pigmented particles in bottled mineral water. Water Res. 2018, 141, 307−316.
(9) Pivokonsky, M.; Cermakova, L.; Novotna, K.; Peer, P.; Cajthaml, T.; Janda, V. Occurrence of microplastics in raw and treated drinking water. Sci. Total Environ. 2018, 643, 1644−1651.
(10) El-Said, W. A.; Cho, H. Y.; Choi, J.-W. SERS Application For Analysis of Live Single Cell. In Nanoplasmonics − Fundamentals and Applications; InTechOpen, 2017.
(11) Perozziello, G.; Candeloro, P.; De Grazia, A.; Esposito, F.; Allione, M.; Coluccio, M. L.; Tallerico, R.; Valpapuram, I.; Tirinato, L.; Das, G.; et al. Microfluidic device for continuous single cells analysis via Raman spectroscopy enhanced by integrated plasmonic nanodimers. Opt. Express 2016, 24, A180.
(12) Ling, L.; Li, Y. Measurement of Raman spectra of single airborne absorbing particles trapped by a single laser beam. Opt. Lett. 2013, 38, 416.
(13) Pan, Y. L.; Wang, C.; Hill, S. C.; Coleman, M.; Beresnev, L. A.; Santarpia, J. L. Trapping of individual airborne absorbing particles using a counterflow nozzle and photophoretic trap for continuous sampling and analysis. Appl. Phys. Lett. 2014, 104, No. 113507.
(14) Uchinokura, K.; Tomoyuki, S.; Matsuura, E. Raman scattering by Silicon. Solid State Commun. 1972, 11, 47−49.
(15) Kravets, V. G.; Kolmykova, V. Y. Raman scattering of light in silicon nanostructures: First- and second-order spectra. Opt. Spectrosc. 2005, 99, 68−73.
(16) Elsayed, A. A.; Erfan, M.; Sabry, Y. M.; Dris, R.; Gaspéri, J.; Barbier, J. S.; Marty, F.; Bouanis, F.; Luo, S.; Nguyen, B. T. T.; et al. A microfluidic chip enables fast analysis of water microplastics by optical spectroscopy. Sci. Rep. 2021, 11, No. 10533.
(17) Ramoji, A.; Galler, K.; Glaser, U.; Henkel, T.; Mayer, G.; Dellith, J.; Bauer, M.; Popp, J.; Neugebauer, U. Characterization of different

substrates for Raman spectroscopic imaging of eukaryotic cells. *J. Raman Spectrosc.* **2016**, *47*, 773−786.

(18) Mikoliunaite, L.; Rodriguez, R.; Sheremet, E.; Kolchuzhin, V.; Mehner, J.; Ramanavicius, A.; Dietrich, D.; Zahn, R. T. The substrate matters in the Raman spectroscopy analysis of cells. *Sci. Rep.* **2015**, *5*, No. 13150.

(19) Oskooi, A. F.; Roundy, D.; Ibanescu, M.; Bermel, P.; Joannopoulos, J.; Johnson, J. Meep: A flexible free-software package for electromagnetic simulations by the FDTD method. *Comput. Phys. Commun.* **2010**, *181*, 687−702.

(20) Xingsheng, X.; Hai, M.; Qijing, Z.; Yunsheng, Z. Properties of Raman spectra and laser-induced birefringence in polymethyl methacrylate optical fibres. *J. Opt. A: Pure Appl. Opt.* **2002**, *4*, 237−242.

(21) Khan, E.; Srivastava, K.; Shukla, A.; Panday, J.; Prajapati, P.; Tandon, P. In *Study of Pharmaceutical Cocrystal Using Experimental and Computational Techniques: An Overview*, Proceedings of International Conference on Perspectives in Vibrational Spectroscopy, 2016.

(22) Du, C. L.; Kasim, J.; You, Y. M.; Shi, D. N.; Shen, Z. X. Enhancement of Raman scattering by individual dielectric microspheres. *J. Raman Spectrosc.* **2011**, *42*, 145.